J Neurophysiol 107: 2594–2603, 2012.
First published February 8, 2012; doi:10.1152/jn.01025.2011.

Receptive field dimensionality increases from the auditory midbrain to cortex

Craig A. Atencio,[1,2] Tatyana O. Sharpee,[3] and Christoph E. Schreiner[1,2]

[1]*The UCSF Center for Integrative Neuroscience and* [2]*Coleman Memorial Laboratory, Department of Otolaryngology-Head and Neck Surgery, University of California, San Francisco; and* [3]*The Salk Institute for Biological Studies and the Center for Theoretical Biological Physics, University of California, San Diego, La Jolla, California*

Submitted 8 November 2011; accepted in final form 8 February 2012

Atencio CA, Sharpee TO, Schreiner CE. Receptive field dimensionality increases from the auditory midbrain to cortex. *J Neurophysiol* 107: 2594–2603, 2012. First published February 8, 2012; doi:10.1152/jn.01025.2011.—In the primary auditory cortex, spectrotemporal receptive fields (STRFs) are composed of multiple independent components that capture the processing of disparate stimulus aspects by any given neuron. The origin of these multidimensional stimulus filters in the central auditory system is unknown. To determine whether multicomponent STRFs emerge prior to the forebrain, we recorded from single neurons in the main obligatory station of the auditory midbrain, the inferior colliculus. By comparing results of different spike-triggered techniques, we found that the neural responses in the inferior colliculus can be accounted for by a single stimulus filter. This was observed for all temporal response patterns, from strongly phasic to tonic. Our results reveal that spectrotemporal stimulus encoding undergoes a fundamental transformation along the auditory neuraxis, with the emergence of multidimensional receptive fields beyond the auditory midbrain.

information; maximally informative dimension; nonlinearity; spectrotemporal receptive field

FOR AUDITORY NEURONS, the spectrotemporal receptive field (STRF) is a complete description of the stimulus preferences of a neuron. The STRF may be approximated as a set of linear filters, or components, that describe the spectrotemporal stimulus selectivity of auditory neurons. The number of filters represents the dimensionality of the STRF (Sharpee et al. 2004). In all layers of primary auditory cortex (AI), STRFs have been shown to have multiple components that capture concurrent processing of disparate stimulus aspects (Atencio et al. 2008, 2009). In contrast, primary visual cortex granular layers predominantly contain simple cells, which can be well described with a single stimulus filter, while extragranular layers are dominated by complex cells, which can only be described with multiple filters. Since the number of filters changes within the visual cortical hierarchy, this indicates that multicomponent receptive fields are constructed within cortex itself. Within AI, however, the situation is different; since neurons in all layers of AI have STRFs with multiple components, it is unknown whether this concurrent, multidimensional processing emerges in AI or whether it is inherited from subcortical stations.

The auditory forebrain comprises the cortex and the thalamus. The midbrain is positioned prior to the forebrain, and it is an obligatory station (Ehret 1997). Signals proceed along the lemniscal pathway from the midbrain, to the thalamus, and then to cortex. Midbrain STRFs have been extensively characterized with single-filter descriptions (Andoni et al. 2007; Escabí and Schreiner 2002; Lesica and Grothe 2008; Rodriguez et al. 2010). It is unknown whether midbrain STRFs can be more completely characterized by using more than one filter.

STRFs can be conceptualized as describing the stimulus filtering that a neuron performs. One approach to estimating STRFs is to calculate the spike-triggered average (STA). The STA is a single filter that may be used to describe spectrotemporal processing (Andoni et al. 2007; Escabí and Schreiner 2002). If the processing of the cell can be captured by one filter, then the STA may be a sufficient descriptor (de Boer and Kuyper 1968). If more than one filter is required, as in visual and auditory cortex (Atencio et al. 2008; Chen et al. 2007; Rust et al. 2005; Touryan et al. 2002), then this model is inadequate. In the auditory midbrain, the main station is the central nucleus of the inferior colliculus (ICC). For the ICC, a single linear filter, in conjunction with a static nonlinearity, may be used to describe some aspects of processing (Andoni et al. 2007; Lesica and Grothe 2008). However, without knowing the number of filters, or stimulus dimensions, that are required to model midbrain function, the adequacy of the model may not be discerned.

Here, to address these questions, we systematically examine spectrotemporal filters in the auditory midbrain. We first address the adequacy of the STA as a functional descriptor for ICC STRFs. Next, we estimate the number of filters that are needed to capture midbrain spectrotemporal processing. We then compare the spectrotemporal processing of midbrain neurons to auditory cortical neurons. This is necessary since more than one filter is present in granular and extragranular layers of auditory cortex, and the demonstration of the existence of multiple filters in earlier stations would constrain the sites of origins of this important processing principle. We conclude by demonstrating the feasibility of spike-triggered analyses for a continuum of ICC temporal response types, from phasic to tonic. Our results reveal that spectrotemporal stimulus encoding undergoes a fundamental transformation between midbrain and forebrain. This transformation is reflected in the emergence of multidimensional receptive fields beyond the auditory midbrain.

METHODS

Electrophysiology. Electrophysiological methods and stimulus design were similar to previous reports (Escabí and Schreiner 2002; Schreiner and Langner 1997). Young adult cats were given an initial dose of ketamine (22 mg/kg) and acepromazine (0.11 mg/kg), and anesthesia was maintained with pentobarbital sodium (Nembutal, 15–30 mg/kg) during the surgical procedure. The animal's temperature was maintained with a thermostatic heating pad. A custom head

Address for reprint requests and other correspondence: C. A. Atencio, 513 Parnassus Ave., HSE 834, Box 0732, San Francisco, CA 94143-0732 (e-mail: craig@phy.ucsf.edu).

holder was used to stabilize the head. Bupivacaine was applied to incision points. Surgery consisted of a tracheotomy, reflection of the soft tissues of the scalp, craniotomy over cortex, and durotomy. The cortex posterior to auditory cortex, and above the ICC, was then aspirated, which allowed for direct visualization of the ICC and later access by a lateral-medial approach (Schreiner and Langner 1997). The tentorium overlaying the ICC was not removed. After surgery, the animal was maintained in an areflexive state with a continuous infusion of ketamine-diazepam (2–10 $mg \cdot kg^{-1} \cdot h^{-1}$ ketamine, 0.05–0.2 $mg \cdot kg^{-1} \cdot h^{-1}$ diazepam in lactated Ringer solution). All procedures were in strict accordance with, and were administered under an experimental protocol approved by, the University of California, San Francisco Committee for Animal Research.

All recordings were made with the animal in a sound-shielded anechoic chamber (IAC, Bronx, NY), with stimuli delivered via a closed speaker system (diaphragms from Stax) that delivered sound through a hollow ear bar that was inserted into the ear canal contralateral to the recording site. Simultaneous extracellular recordings were made with multichannel gold-plated silicon recording probes (kindly provided by the University of Michigan Center for Neural Communication Technology). The probes contained 16 linearly spaced recording channels, with each channel separated by 0.15 mm. The impedance of each channel was 4–5 MΩ. Probes were positioned orthogonally with a microdrive (David Kopf Instruments, Tujunga, CA).

Neural traces were band-pass filtered between 600 and 6,000 Hz and were recorded to disk with a Neuralynx Cheetah A/D system at sampling rates between 18 and 27 kHz. The traces were sorted off-line for single units with a Bayesian spike-sorting algorithm (Lewicki 1994).

After spike sorting and analysis, neurons were determined to be in the central nucleus of the ICC by analyzing responses to pure tones and ripple stimuli (Merzenich and Reid 1974; Schreiner and Langner 1997). The ICC was identified with physiological criteria: As recording depth increased, there was an accompanying increase in characteristic frequency with pure tones and in best frequency with STRFs (see below for analysis procedures).

Stimulus. For any recording position, neurons were probed with pure tones and then with a 20-min dynamic moving ripple (DMR) stimulus. Pure tones were 50 ms in duration, had 5 ms cosine-squared onset/offset ramps, and were presented every 300 ms. The frequency and level of each tone were chosen from 45 frequencies and 15 levels, resulting in a set of 675 different tones. The set was presented in pseudorandom sequence (Schreiner and Sutter 1992). Level steps were 5 dB and covered a range of 70 dB. Frequencies were logarithmically spaced and encompassed the frequency preferences of encountered neurons. For the DMR stimulus, the maximum spectral modulation frequency was 4 cyc/oct, and the maximum temporal modulation frequency was 500 cyc/s (Escabí and Schreiner 2002). Maximum modulation depth of the spectrotemporal envelope was 40 dB. Mean intensity was set at 30–50 dB above the mean pure-tone threshold.

Analysis. Data analysis was carried out in MATLAB (MathWorks, Natick, MA). We used the reverse correlation method to derive the average spectrotemporal stimulus envelope preceding a spike (STA) (Aertsen and Johannesma 1981; deCharms et al. 1998; Escabí and Schreiner 2002).

To obtain the maximally informative dimensions (MIDs), we followed previously reported methodologies (Sharpee et al. 2004, 2006). To find relevant stimulus dimensions, we searched through the stimulus space for those dimensions that maximized the mutual information between the stimulus and the spiking response. The first MID (MID1) is the direction in stimulus space that maximizes the mutual information between the stimulus and the response. The second MID (MID2) was then found as the dimension in the stimulus space that, together with the first MID, further maximized the information. The mutual information between projections onto individual filters, v, and single spikes was computed according to

$$I(v) = \int \mathrm{d}x P_v(x|\mathrm{spike}) \log_2 \left[\frac{P_v(x|\mathrm{spike})}{P_v(x)} \right]$$

where x represents projections onto the relevant dimension, v. $P_v(x)$ is the distribution of projections for all presented stimuli. $P_v(x|\mathrm{spike})$ is the distribution of projections for only those stimuli that led to a spike. The filter v was either MID1 or MID2. The one-dimensional input/output nonlinearity was calculated via

$$P_v(\mathrm{spike}|x) = P(\mathrm{spike}) \frac{P_v(x|\mathrm{spike})}{P_v(x)}$$

where $P(\mathrm{spike})$ is the average firing rate of the neuron.

The mutual information between single spikes and both MIDs was calculated as

$$I(\mathrm{MID1}, \mathrm{MID2}) = \int\int \mathrm{d}x_1 \mathrm{d}x_2 P(x_1, x_2|\mathrm{spike}) \log_2 \left[\frac{P(x_1, x_2|\mathrm{spike})}{P(x_1, x_2)} \right]$$

where x_1 and x_2 represent the projections of the stimulus onto the first and second MIDs, respectively. The two-dimensional nonlinearity was calculated via

$$P(\mathrm{spike}|x_1, x_2) = P(\mathrm{spike}) \frac{P(x_1, x_2|\mathrm{spike})}{P(x_1, x_2)}$$

All estimates of relevant stimulus dimensions (STA, MID1, MID2) were computed as an average of four jackknife estimates. Each jackknife estimate was computed by using a different ¾ of the data (the training data set), and thus leaving a different ¼ of the data as a test data set. Information values were calculated using different fractions of the test data set for each neuron. To accomplish this, the information values were calculated over the first 80%, 90%, 92.5%, 95%, 97.5%, and 100% of the test data set. The information calculated from these data fractions was plotted against the inverse of the data fraction percentage (1/80, 1/90, etc.). We extrapolated the information values to infinite data set size by fitting a line to the plot and taking the y-axis intersect as the information value for unlimited data size (Brenner et al. 2000; Strong et al. 1998; Treves and Panzeri 1995).

From the STA and MID1, we obtained the latency, best frequency (BF), bandwidth (BW), and spectral tuning. To obtain the parameters, the filter was summed across time or frequency, which produced the frequency or time marginals, respectively. The time or frequency axis for each marginal was then upsampled 500 times (using MATLAB function linspace.m), and the marginals were interpolated (using MATLAB function interp1.m with "spline" option). Latency was defined as the peak in the time marginal. BF was defined as the peak in the frequency marginal, and BW was the width of the distribution at 25% of the peak height. Spectral tuning, defined as the quality factor Q, was calculated from the BF and BW via Q = BW/BF.

The similarity between filters was calculated with the Pearson correlation coefficient, r, defined as

$$r = \frac{\sum_i \sum_j A(i,j)B(i,j)}{\sqrt{\sum_i \sum_j A(i,j)A(i,j)} \sqrt{\sum_i \sum_j B(i,j)B(i,j)}}$$

where A and B are matrices and may be either the STA or MID1. The similarity ranges between +1 and −1 and is a measure of the spectrotemporal correlation between the two filters.

The temporal evolution of pure-tone responses was evaluated with the phasic-tonic index (PTI):

$$\mathrm{PTI} = N_E/(N_B + N_E) = N_E/N_T$$

where N_B is the number of spikes during the first half of the stimulus, N_E is the number of spikes during the last half of the stimulus, and N_T

is the sum of N_B and N_E. For purely phasic neurons the PTI is 0, while for tonic responses the PTI is ~0.5. The PTI includes data from all pure-tone presentations; thus it may include responses that are phasic at low sound levels or at the edge of a neuron's frequency response area. In this manner, the PTI is a conservative measure.

The MID1 contribution was defined as $100 \cdot I(\text{MID1})/I(\text{MID1, MID2})$. The STA and MID1 were compared using the STA sufficiency metric, defined as $100 \cdot I(\text{STA})/I(\text{MID1})$. For both measures we used the information values from the extrapolation procedure.

We also followed previous work and computed a response precision index (RPI) for each neuron using the relation $\text{RPI} = [\max(\text{STA}) - \min(\text{STA})]/fr\sqrt{8}$, where max(STA) and min(STA) are the maximum and minimum values in the STA and *fr* is the average firing rate (Escabí and Schreiner 2002). The RPI measures the temporal precision of a neuron by comparing the difference between the maximum and minimum in the estimated STA to the expected theoretical difference for stimuli that are perfectly aligned (Escabí and Schreiner 2002). The RPI ranges from 0 (not temporally precise) to 1 (temporally precise).

RESULTS

The ICC is an obligatory computational hub in the central auditory system (Aitkin 1986; Ehret 1997). Information from brain stem nuclei, such as the superior olivary complex and cochlear nucleus, converges onto the ICC (Oliver 2005; Schofield 2005). The projections to the ICC are localized into specific topographic domains (Malmierca et al. 2005; Oliver 2000; Oliver et al. 1995; Schofield 2005). Although our knowledge of these projection patterns is extensive, our understanding of ICC spectrotemporal processing is less comprehensive.

Our goal in this study was to estimate ICC STRFs. To characterize ICC neurons, we used two types of stimuli: pure tones and a dynamic, broadband sound. In the ICC, the temporal response pattern to pure tones fell along a gradient, from tonic to phasic. For tonic responses, vigorous discharges occurred throughout the stimulus duration (Fig. 1).

The responses can be more fully appreciated with the poststimulus time histogram (PSTH). The PSTH was estimated by including responses to every pure-tone frequency-intensity combination. For predominantly tonic cells, the response duration was tightly locked to the pure-tone duration (Fig. 1; pure-tone duration of 50 ms indicated by gray boxes). Additionally, tonic neurons often had few discharges after 150 ms, which is 100 ms after tone offset, further indicating effective stimulus entrainment (Fig. 1, *A* and *B*).

Tonic responding neurons responded vigorously to the DMR. Although the DMR has no well-defined onset, tonic neurons exhibited high discharge rates in response to this continuous stimulus. Spike rates in response to the DMR often exceeded 20 spikes/s [median = 12.5, median absolute deviation (m.a.d.) = 9.4]. Despite these high rates, we were able to obtain the STA from DMRs for tonic responding neurons (Fig. 1).

A wide variety of temporal responses were found in the midbrain. Responses could be highly tonic with little background activity (Fig. 1, *A–C*); they could be tonic with much background activity (Fig. 1, *D* and *E*); in some cases they were onset with a sustained component (Fig. 1*F*); and in other cases responses were highly phasic (Fig. 1*G*). In all cases, we were able to estimate well-defined STAs (Fig. 1). Thus the phasic-tonic nature of the responses had no bearing on our ability to utilize spike-triggered averaging techniques.

The temporal response type of a neuron was not directly related to the structure of the STA. For tonic responses, diverse STA patterns were observed: excitation present without inhibition (Fig. 1*A*; excitation: red subfields; inhibition: blue subfields); excitation followed by inhibition (Fig. 1*D*); excitation flanked by inhibition in time and frequency (Fig. 1*E*); or excitation accompanied by strong spectral sidebands (Fig. 1*F*). Phasic neurons similarly exhibited temporal and spectral inhibitory sidebands (Fig. 1*G*). The overall impact of temporal response profiles on STRFs is quantified further below.

Single-dimensional STRFs. The receptive field estimated by the STA represents a single feature dimension in the spectrotemporal stimulus space. The STA captures the average stimulus feature that accounts for a neuron's response. Another approach that may be used to obtain the STRF is MID analysis. In this framework, an STRF, or linear filter, is estimated by maximizing the mutual information between the stimulus and the spiking response (Atencio et al. 2008, 2009; Sharpee et al. 2004). The filter is calculated by an iterative process, and the result is the stimulus feature that best describes the acoustic pattern that drives the neuron. The resulting filter, which accounts for the most mutual information, is the first MID (MID1). MID1 is an unbiased estimate since the iteration process removes the effects of stimulus correlations, which can confound STRF estimates when the stimulus ensemble contains higher-order correlations (Sharpee et al. 2004). For every neuron with an STA we were also able to calculate an MID1 (Fig. 2*C*). The STAs and MID1s were very similar, indicating that both approaches are adequate descriptors of a linear, single-dimensional STRF (Fig. 2, *A* and *C*).

The MID analysis may be expanded so that we can estimate the potential contributions of a second, independent filter, MID2. The presence of an MID2 further maximized the mutual information between the stimulus and the response (Fig. 2*E*). MID2s in the ICC, however, hardly increased the total information captured by the combined application of the MIDs and seldom revealed structured excitatory or inhibitory subfields (see below).

STA and MID1 example nonlinearities. For each spectrotemporal filter, a nonlinear function may be calculated that describes the firing rate of the neuron as a function of the similarity between the stimulus and the filter. This static, time-independent function is termed a nonlinearity. This nonlinearity represents a rule that describes how the neuron will respond, given the similarity between the stimulus and the filter. STA (Fig. 2*B*) and MID1 (Fig. 2*D*) nonlinearities were similar, with each having an asymmetric structure. Thus, when the stimulus is negatively correlated with the filter, the response of the neuron decreases below the mean driven firing rate (Fig. 2; dashed lines indicate mean rate). As the similarity increases, the response strength of the neuron increases. For some nonlinearities, the response rate plateaus (Fig. 2, 3rd row), although for most the response is highly monotonic. MID2 nonlinearities were less stereotyped in structure, and often did not deviate from the mean driven response rate (Fig. 2*F*).

To estimate how well the STA approximates MID1, the STA and MID1 filters and nonlinearities may be compared. We first compared basic parameters from each filter. The response

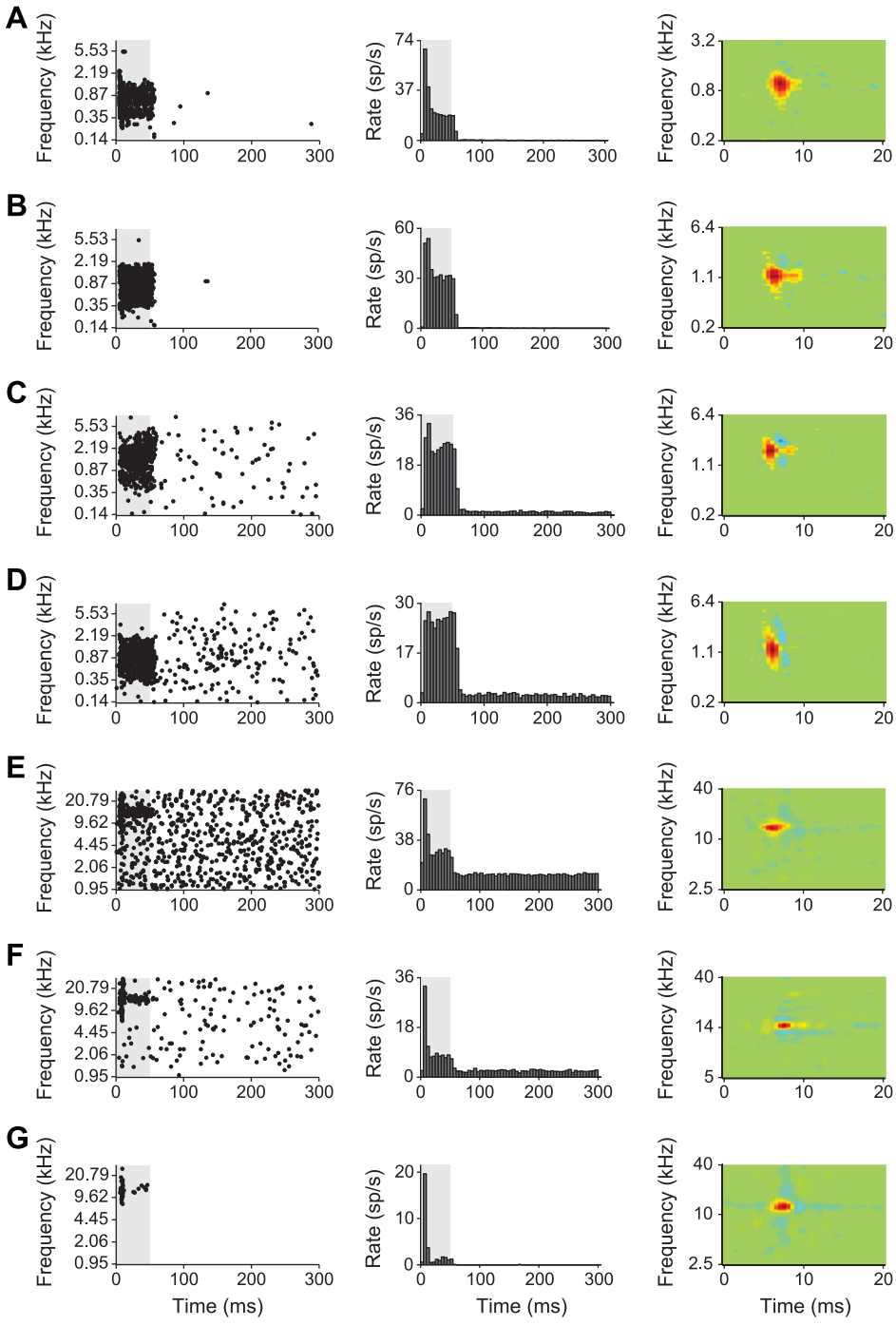

Fig. 1. Response patterns and spike-triggered averages (STAs) for midbrain neurons. Each row (*A–G*) represents 1 neuron. *Left*: spike raster for pure tones. Raster responses are shown for the sound level at which the ripple stimulus was presented. Gray boxes indicate the tone stimulus duration. *Middle*: poststimulus time histogram (PSTH) across all pure-tone presentation sound levels. *Right*: STA.

latency was highly similar for the STA and MID1 (Fig. 3*A*; $r = 0.995$, $P < 0.001$, *t*-test). BF was even more highly correlated (Fig. 3*B*; $r = 0.999$, $P < 0.001$, *t*-test). Additionally, the BW of each filter was matched (Fig. 3*C*; $r = 0.982$, $P < 0.001$, *t*-test). Finally, the spectral tuning of each filter, defined as the quality factor Q (= BW/BF), was also significantly correlated across STA and MID1 filters (Fig. 3*D*; $r = 0.975$, $P < 0.001$, *t*-test).

For the STA and MID1, we also compared the global structure of the filters and nonlinearities. The correlation between the filter structure was never below 0.8 (Fig. 3*E*; median = 0.948, m.a.d. = 0.016), further indicating a strong agreement between MID1 and the STA. The correlation between the nonlinearities was also high (Fig. 3*F*; median = 0.905, m.a.d. = 0.087), implying that the STA is a sufficient approximation to MID1.

The performance of the STA and the MIDs may be estimated by calculating the mutual information. We measured the performance in the midbrain and then compared this to the performance in AI, using previously published data (Atencio et al. 2008). We used mutual information because it is an objective measure of the stimulus-response relationship that has been used extensively to evaluate neural processing. For midbrain neurons, the information provided by MID1 was highly similar to that provided by the STA, indicating that the performance of each STRF model was nearly indistinguishable (Fig. 4*A*; $P = 0.481$, rank sum test). By contrast, for cortical

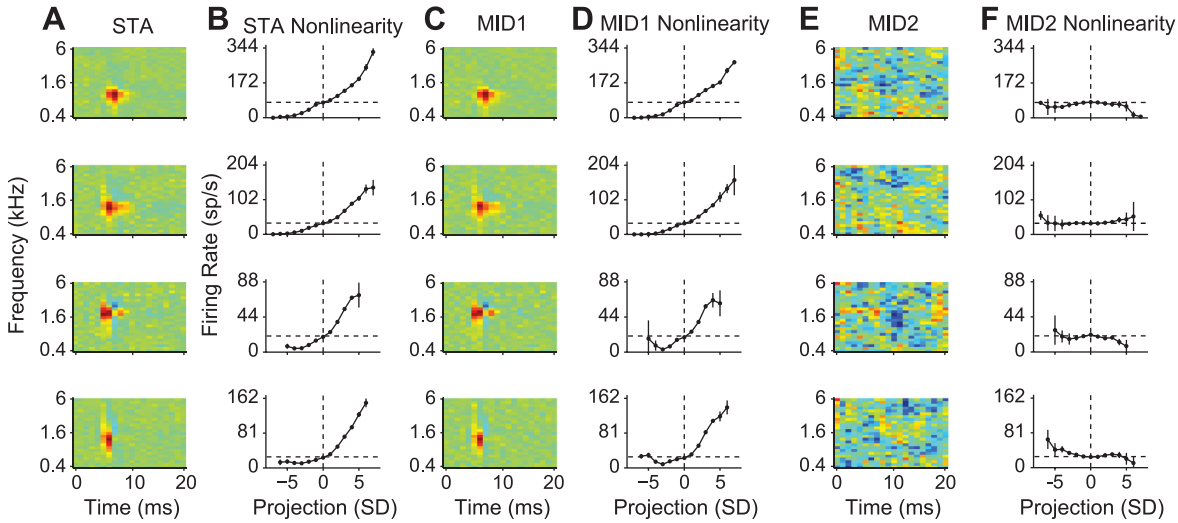

Fig. 2. STAs, maximally informative dimensions (MIDs), and nonlinearities. Each row represents the filters and nonlinearities for 1 neuron. *A* and *C*: STAs and MID1s have similar filter structure. *E*: MID2s are less structured. *B* and *D*: STA and MID1 nonlinearities are similar. Dashed horizontal lines indicate mean firing rate. *F*: MID2 nonlinearities show little deviation from the mean firing rate. For nonlinearities, increasing similarity values indicate increasing correlation between filter and stimulus.

neurons, there was much more scatter between the two estimates, and the STA information was often less than the MID1 information ($P < 0.001$, rank sum test). The ratio of the STA information to the MID1 information is the STA sufficiency. In the midbrain the STA sufficiency was often ~80%, while in the cortex the distribution was not dominated by such high values (Fig. 4*B*).

Multidimensional STRFs. One of the main advantages of the MID analysis is that a second filter, MID2, may be estimated (Atencio et al. 2008, 2009). This second MID defines an additional stimulus-based dimension that, in conjunction with MID1, further maximizes the mutual information between the stimulus and the response (Fig. 2*E*).

MID2s in ICC neurons seldom had discernible structures, and combining both filters did not add substantial explanatory

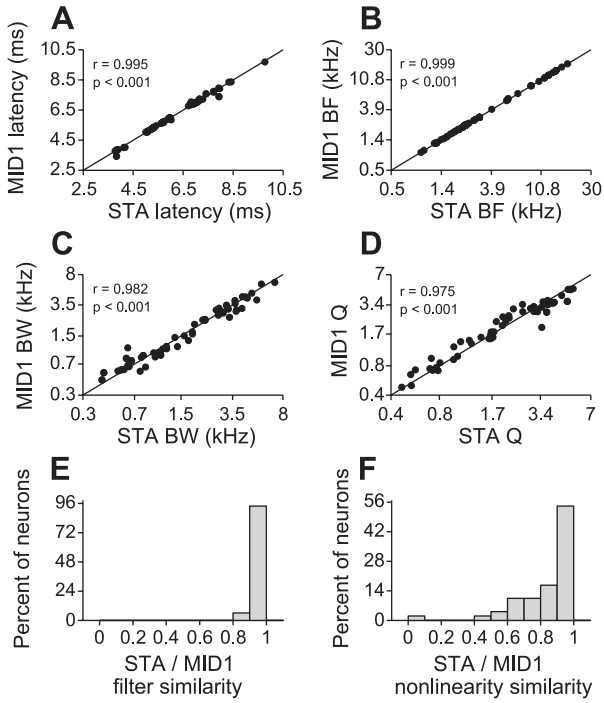

Fig. 3. Comparison between STA and MID1 filters and nonlinearities. *A*: latencies for STA and MID1 were highly similar ($r = 0.995$, $P < 0.001$, *t*-test). *B*: best frequencies (BF) for STA and MID1 were highly similar ($r = 0.999$, $P < 0.001$, *t*-test). *C*: excitatory bandwidths (BW) of the filters were highly similar ($r = 0.982$, $P < 0.001$, *t*-test). *D*: spectral tuning (Q = BW/BF) was highly similar ($r = 0.975$, $P < 0.001$, *t*-test). *E*: correlations between STA and MID1 filters were high [median = 0.948, median absolute deviation (m.a.d.) = 0.016]. *F*: correlations between STA and MID1 nonlinearities were also high (median = 0.905, m.a.d. = 0.087). In *A*–*D*, diagonal lines represent the unity relationship.

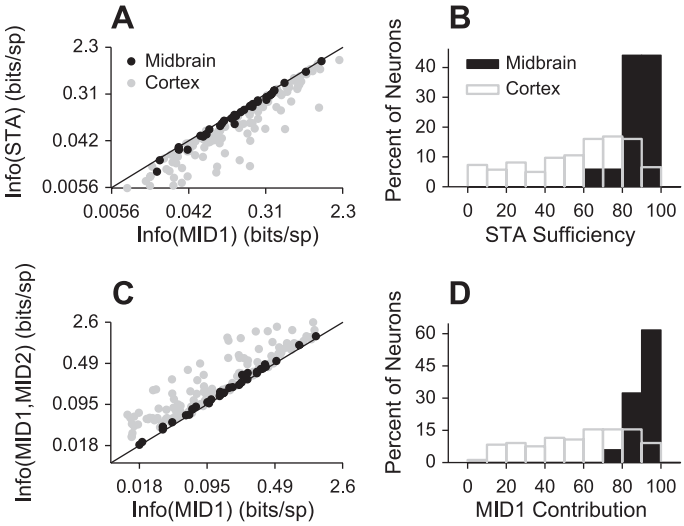

Fig. 4. STA and MID information analysis in midbrain and primary auditory cortex. *A*: STA and MID1 information were highly similar in midbrain and moderately similar in cortex. *B*: STA sufficiency [100·Info(STA)/Info(MID1)] was greater in the midbrain than in the cortex ($P < 0.001$, rank sum test). *C*: MID1 information was similar to the joint MID1 and MID2 information for all neurons in midbrain and less similar in cortex. *D*: MID1 contribution [100·Info(MID1)/Info(MID1,MID2)] was greater in the midbrain, indicating that the MID1 information approximated the 2-filter information to a much greater degree than in cortex ($P < 0.001$, rank sum test). In *A* and *C*, diagonal lines represent the unity relationship.

power over either the STA or the MID1 single-dimensional filter model.

Comparing the MID1 information values to the joint MID1 and MID2 information allows us to estimate the dimensionality of the STRFs in the ICC and the cortex (Fig. 4*C*). If the joint information is significantly greater than the MID1 information, then more than one MID, or stimulus feature dimension, is required to adequately describe ICC processing. Alternatively, when the MID1 information is approximately equal to the joint MID1 and MID2 information, then the second filter, MID2, provides little additional information. For midbrain neurons, the MID1 information was statistically indistinguishable from the joint MID1 and MID2 information (Fig. 4*C*; $P = 0.594$, rank sum test). By contrast, in the cortex, the MID1 information was significantly less than the joint filter information ($P < 0.001$, rank sum test).

The ratio of the MID1 information to the joint MID1 and MID2 information may be formed, and is termed the MID1 contribution (Fig. 4*D*). Across ICC neurons, MID1 accounted for >80% of the information in a two-MID model; this indicates that MID1 by itself may be quite adequate to describe the spectrotemporal processing of ICC neurons. The MID1 contribution fell below 75% for only one neuron (Fig. 4*D*). This result is in striking contrast to the much lower contribution values reported for AI (Atencio et al. 2008, 2009). Thus, for all neurons we encountered, the processing in the ICC may be accounted for by a single filter, while in the auditory cortex more than one filter may be required.

Response measures. One of the goals of our study was to determine the information processing of the different temporal response types found in the ICC. To characterize the responses of ICC neurons and their impact on STRF estimation, we utilized two metrics from the DMR responses and one from the pure-tone responses. The first DMR metric was firing rate (the number of spikes divided by the duration of the DMR). We encountered a broad range of firing rates, ranging up to 70 spikes/s over the duration of the DMR (Fig. 5*A*). These values are consistent with previous definitions of sustained responses in the auditory cortex: a firing rate >5 spikes/s during both the first and the second half of the stimulus (Wang et al. 2005). The second DMR metric was the RPI, which measures a neuron's temporal precision (see METHODS). RPIs were distributed over a broad range (Fig. 5*B*; median = 0.114, m.a.d. = 0.049), which was consonant with previously described midbrain properties (Escabí et al. 2005).

The temporal evolution of pure-tone responses was evaluated with the PTI. For purely phasic neurons the PTI is 0, while for tonic responses the PTI is ~0.5. The responses of ICC neurons were distributed across a broad range of PTI values (Fig. 5*C*; median = 0.426, m.a.d. = 0.048), and sustained portions were frequent, accounting for a mean PTI near 0.5.

Firing rate and the RPI were hyperbolically related, with the lowest firing rates correlated with high RPI values (Fig. 5*D*; $r = -0.428$, $P = 0.0005$). The PTI was weakly correlated with firing rate, indicating that sustained responses could be recovered over a range of response strengths (Fig. 5*E*; $r = 0.326$, $P = 0.0097$). Finally, the RPI was not correlated with the PTI; thus tonic and phasic responses occurred across a wide range of RPIs (Fig. 5*F*; $r = -0.135$, $P = 0.295$).

Information analysis for response metrics. After we characterized the response types of ICC neurons we then related the types to receptive field processing. The information results for the STA and the MIDs generalized across response type in the ICC. The STA sufficiency was high regardless of the firing rate of ICC neurons, indicating that the STA information approximated that of MID1 across all response strengths (Fig. 6*A*; $r = -0.165$, $P = 0.352$). Additionally, the STA sufficiency was not affected by response precision; it was similar across different RPIs (Fig. 6*B*; $r = 0.285$, $P = 0.103$). Finally, the STA sufficiency was independent of either phasic or tonic response behavior (Fig. 6*C*; $r = 0.053$, $P = 0.768$).

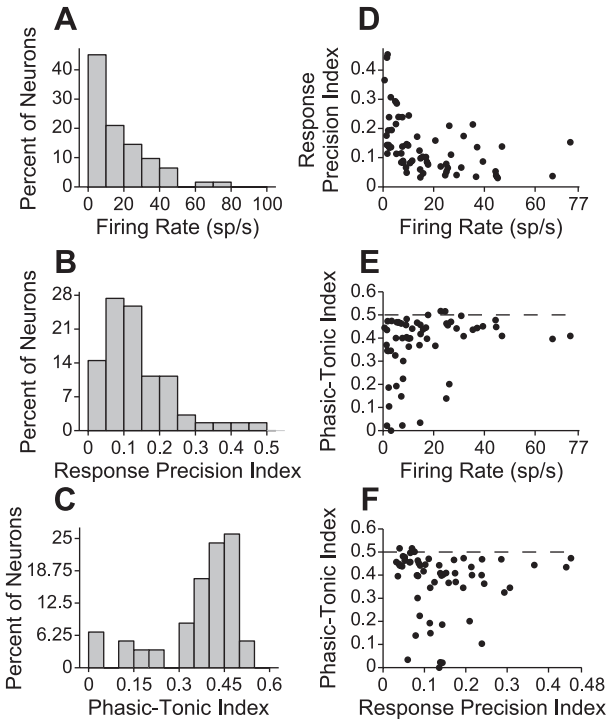

Fig. 5. Phasic-tonic index (PTI), response precision index (RPI), and firing rate of midbrain neurons. *A*: firing rate distribution for inferior colliculus (ICC) neurons (median = 12.5, m.a.d. = 9.4). *B*: RPI distribution (median = 0.114, m.a.d. = 0.049). *C*: PTI distribution (median = 0.426, m.a.d. = 0.048). *D*: RPI vs. firing rate ($r = -0.428$, $P = 0.0005$, *t*-test). *E*: PTI vs. firing rate ($r = 0.326$, $P = 0.0097$, *t*-test). Dashed line indicates the PTI value for an ideally tonic neuron (equal numbers of spikes throughout the stimulus duration). *F*: PTI vs. RPI ($r = -0.135$, $P = 0.295$, *t*-test).

The MID1 contribution measures the dimensionality of ICC processing, and it achieved similarly high values for the three response metrics. For firing rate, the MID1 contribution was not dependent on the response strength of the neuron (Fig. 6*B*; $r = 0.231$, $P = 0.188$). The response precision of the neuron was also not correlated with model complexity (Fig. 6*D*; $r = 0.049$, $P = 0.784$). Finally, the PTI was moderately correlated with the MID1 contribution (Fig. 6*F*; $r = 0.484$, $P = 0.004$). However, for almost all neurons, no matter the PTI, the MID1 contribution was >75%. Therefore, regardless of response strength or temporal response pattern, MID1 is an appropriate model for the spectrotemporal processing of ICC neurons.

Information analysis in ICC and primary auditory cortex. For ICC neurons, a single filter—combined with an appropriate input/output nonlinearity—is sufficient to describe spectrotemporal processing. One filter is appropriate regardless of the response strength; it is also sufficient for phasic-to-tonic response patterns. This finding contrasts with those from AI, where multiple filters are present in granular (~600–1,100

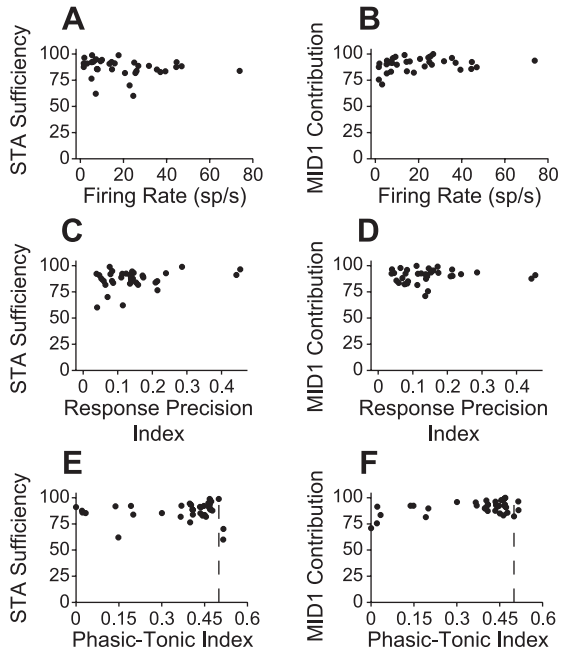

Fig. 6. Comparison between response metrics and information in the midbrain. *A*: STA sufficiency compared with firing rate for midbrain cells. *C*: STA sufficiency vs. RPI. *E*: STA sufficiency vs. PTI. For all metrics the STA sufficiency was high. *B*: MID1 contribution vs. firing rate. *D*: MID1 contribution vs. RPI. *F*: MID1 contribution vs. PTI. For all metrics, MID1 information was highly similar to the joint MID1 and MID2 information.

μm) and nongranular layers (Atencio et al. 2009; Huang and Winer 2000; Mitani et al. 1985; Rouiller et al. 1991; Winer 1984). To compare the midbrain and the cortex, we used previously published data from AI (Atencio et al. 2008, 2009). When we compared the STA sufficiency distributions, we found that the midbrain population diverged significantly from the cortical population. Compared with both cortical granular and nongranular layers, the ICC population was significantly shifted toward higher values [Fig. 7*A*; granular layers vs. midbrain: $P < 0.001$, Kolmogorov-Smirnov (KS) test; nongranular layers vs. midbrain: $P < 0.001$, KS test]. Thus a single-filter characterization is sufficient for the ICC but not for AI granular (thalamic input) and nongranular layers. In addition, midbrain STAs were better approximations to MID1s than cortical STAs to MID1s (Fig. 7*C*; ICC: median = 89.7, m.a.d. = 5.94; AI: median = 63.1, m.a.d. = 18.4; rank sum test, $P < 0.001$).

Furthermore, the strength of the first MID, relative to a combined first and second MID model, was substantially different between midbrain and cortex (Fig. 7, *B* and *D*). The midbrain had a stronger relative MID1 compared with either granular or nongranular data (Fig. 7*B*; granular layers vs. midbrain: $P < 0.001$, KS test; nongranular layers vs. midbrain: $P < 0.001$, KS test). This indicates that the multiple-filter model of AI is not passively received ("inherited") from midbrain processing. At the population level, the MID1 contribution was much greater in the ICC than in AI (ICC: median = 92.0, m.a.d. = 4.58; AI: median = 62.4, m.a.d. = 20.4; rank sum test, $P < 0.001$). Thus the second MID contributes much more to information processing in AI than in the ICC. Therefore, the number of stimulus dimensions needed to describe AI neurons is substantially different from the number needed for the midbrain.

DISCUSSION

A single stimulus filter dominates the spectrotemporal processing in the auditory midbrain, whereas primary cortical neurons in all cortical layers are best characterized by at least two filters (Atencio et al. 2008, 2009). This implies that the nature of receptive fields undergoes a fundamental transformation from subcortical to cortical stations. We established this result in several ways.

First, for each ICC response type we encountered, whether phasic or tonic, a single filter accounted for the overwhelming majority of the conveyed stimulus information. Additionally, the single-filter description held irrespective of the response metric we employed, indicating that neither levels of firing rate nor the degree of response precision conflicts with this result. Therefore, the single-filter description likely generalizes across the population of midbrain cells.

Second, the STA was an adequate descriptor of spectrotemporal ICC processing. For cells with only one relevant stimulus dimension, and with appropriate stimuli, the STA and MID descriptions should be similar. On the basis of filter similarity and information, the ICC STA was nearly equivalent to MID1. Thus the STA and MID1 correspond to the same stimulus dimension that accounts for ICC responses. This is striking, since the STA is a much simpler measure than an MID, both to compute and to interpret. It implies that simple reverse correlation may be used to obtain an unbiased receptive field estimate for the ICC.

Third, the single feature selectivity of the ICC was confirmed by assessing the impact of a second MID. The MID analysis produced a second MID for ICC neurons. However, the filter shape was diffuse, and the information contributed by

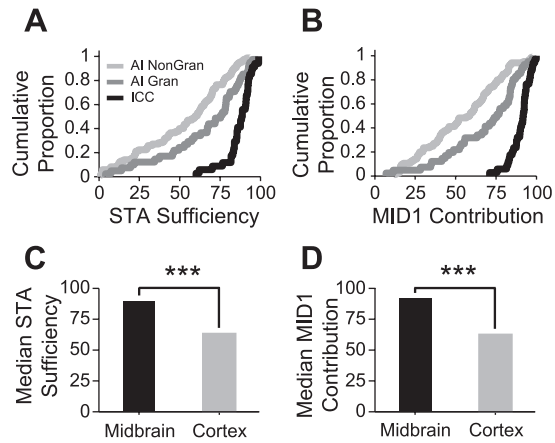

Fig. 7. Midbrain and primary auditory cortex (AI) MID summary. *A*: cumulative distribution for STA sufficiency. Compared with cortical granular (Gran) and nongranular (NonGran) layers, midbrain STA information more closely approximated the MID1 information [granular layers vs. midbrain: $P < 0.001$, Kolmogorov-Smirnov (KS) test; nongranular layers vs. midbrain: $P < 0.001$, KS test]. *B*: cumulative distribution for MID1 contribution. Compared with cortex, in the midbrain MID1 accounted for a greater percentage of the joint MID1 and MID2 information (granular layers vs. midbrain: $P < 0.001$, KS test; nongranular layers vs. midbrain: $P < 0.001$, KS test). *C*: median STA sufficiency values. Midbrain values were higher than cortical values (***$P < 0.001$, rank sum test). *D*: median MID1 contribution values. Midbrain values were higher than those in cortex (***$P < 0.001$, rank sum test).

MID2 was negligible. By contrast, in AI, second MIDs with significant information contributions and reliable filter shapes were encountered for the vast majority of neurons in both the thalamic input/granular layers and the output/extragranular layers. The existence of multiple filters in the cortical input layers permits the possibility that the multiple-filter property is generated before AI. However, since the number of filters required to describe midbrain responses is different from that in the cortical input layers, this eliminates the possibility that cortical processing properties are inherited from collicular neurons. The possibility of the emergence of multiple spectrotemporal filters in thalamic neurons is still feasible.

Transformations in central auditory system. For sound processing, there are relatively few established transformations along the ascending central auditory pathway. The most widely recognized processing change is the transition from a temporal to a more rate-based coding scheme. For example, phase-locking to the stimulus fine structure degrades as information proceeds from lower to higher stations (Johnson 1980; Kuwada et al. 1984; Liu et al. 2006; Lu et al. 2001; Winter and Palmer 1990). Also, the highest temporal modulation frequency to which neurons may respond with a temporal code decreases across the populations (Joris et al. 2004).

Our analyses established a further transformation that is fundamentally different from those that are related to temporal coding: The manner in which spectrotemporal information is processed changes from midbrain to cortex. By showing that the number of STRF components increases from the ICC to AI, we have uncovered one of the first fundamental receptive field transformations in the central auditory system: the emergence of multidimensional receptive fields in the auditory forebrain. The forebrain is composed of both the auditory cortex and the auditory thalamus (medial geniculate body). We can only speculate at this time on whether multidimensional receptive fields will be found in the thalamus. We do note that the thalamus, like the ICC, has a laminated structure (Morest 1965). Additionally, thalamic circuitry appears to be more similar to that in the ICC than to the cortex, and the number of cell types is also restricted relative to cortex (Winer 1992). Given these admittedly cursory considerations, we expect that thalamic receptive field processing will be more similar to that in ICC than that in AI. Thus, if future work shows that the thalamus can also be sufficiently described with a single filter, then the multiple-filter model for AI neurons, which is present in all cortical layers, would be an emergent feature of the cortical circuit itself.

The change from single to multiple feature selectivity is conceptually significant since it indicates that even though the ICC is an obligatory processing station for auditory information, further emergent changes take place in the forebrain. The conclusiveness of previous characterizations of central processing principles has often been hampered, since it has been difficult to demonstrate and isolate truly emergent properties in AI with simple stimuli. A creation of de novo receptive field properties had not been described for AI. This contrasts with primary visual cortex, where orientation selectivity and binocularity first emerge in the thalamic recipient layer 4, and therefore experiments in that modality can be tailored to understand the development, plasticity, and circuitry governing the emergence of functional parameters. Since our findings in the ICC implicate the auditory forebrain as the site of emergent processing, experiments may now be performed to understand how this processing may be enhanced, degraded, or modified in accordance with approaches including network manipulations, development, learning, and/or attention. Therefore, the function of the auditory cortical circuit may be examined, and changes to the circuit itself may be correlated with specific aspects of receptive field processing and with the implementation of task-specific algorithms.

Previous results. Spike-triggered analysis techniques have been successfully applied to ICC neurons. Nonlinear receptive field aspects have been revealed with uncorrelated noise and DMR stimulation (Escabí and Schreiner 2002). STRFs have also been moderately successful in linearly predicting midbrain responses (Andoni et al. 2007; Lesica and Grothe 2008). In the bat ICC, the STRF from spike-triggered averaging can predict frequency modulation preferences (Andoni et al. 2007). The structure of the STRF was found to be highly correlated with frequency modulation direction selectivity. In the gerbil ICC, a complex rain sound has been used to calculate the STRF (Lesica and Grothe 2008). Here, the STRF was estimated with ridge regression, which is a modified extension of the STA (Lesica and Grothe 2008). The filter estimated from this approach was relatively successful in predicting the temporal spiking behavior of gerbil ICC cells. Finally, in the awake rhesus monkey ICC, STRFs were used to predict responses to noise and vocalizations (Versnel et al. 2009). Here STRFs were estimated from static ripple stimuli. Like the DMR, static ripple stimuli are characterized by two parameters, a temporal and a spectral modulation frequency. Unlike the DMR, the two parameters do not vary with time (Klein et al. 2000). The predictive power of the rhesus monkey STRFs was probably underestimated for two reasons. First, the predictions were not compared to the inherent variance in the neural response (Hsu et al. 2004; Sahani and Linden 2003). Second, the study did not use a static nonlinearity, which is known to increase predictive power (Sharpee et al. 2008). Therefore, our study provides a context in which to view these successes, since our findings indicate that, for some stimuli, ICC cells can be adequately described with a single filter followed by a customized static input/output nonlinearity.

Implications for receptive field analysis. We were able to apply spike-triggered techniques to ICC neurons because neural systems satisfy fundamental systems analysis requirements. Theoretically, a nonlinear dynamic system may be described by a Volterra series if the system is nonchaotic, nonoscillatory, and time-invariant and has finite memory (Boyd and Chua 1985; Marmarelis 2004; Westwick and Kearney 1998). Importantly, the Volterra series can be formulated in the linear-nonlinear (LN) model configuration (Palm 1979). The LN model, which is also termed a Wiener-Bose or parallel-cascade model, is a bank of linear filters followed by a static nonlinearity (Korenberg 1991; Marmarelis 1997, 2004). The STA/MID approach, with accompanying nonlinearities, falls under the general framework of the LN model (Schwartz et al. 2006). The only stimulus requirement for these models is that the statistics of the stimulus be broad enough to effectively cover the stimulus preferences of the neuron (Marmarelis and Marmarelis 1978; Marmarelis 2004). Appropriate techniques may then be used to correct for stimulus correlations and to estimate the proper number of filters (Sharpee et al. 2004). Hence, for auditory neurons, we can calculate STRFs if the stimulus

modulates the firing rate. Thus spike-triggered analyses can also be used to characterize tonic neural responses. For a dynamic stimulus, only when the firing rate does not modulate in response to changing stimulus features will the STRF procedure not work. However, in this case, the neuron's response is not informative. In short, if the response varies when stimulus features vary, then judiciously applied spike-triggered approaches may be useful.

Further considerations. Like every approach, the scope of our results are necessarily constrained by the details and assumptions of our methodology. In this regard there are important issues to consider. First, we employed the DMR stimulus because it contains temporal and spectral modulations, which are important components of natural sounds. Natural sounds may have other features that are not modeled by the DMR, and thus calculating MIDs with naturalistic stimuli may lead to moderately different results (David et al. 2009; Singh and Theunissen 2003). Second, how the DMR is represented may be pertinent. Although the neurons themselves responded to the entire stimulus waveform, we estimated filters with the spectrotemporal envelope. The stimulus waveform fine structure is a richer representation than the envelope. Previous work has shown that auditory cortical neurons may indeed be sensitive to stimulus fine structure (Elhilali et al. 2004). Sensitivity to fine temporal features may be even more pronounced in the ICC, which has better temporal resolution than auditory cortex (Joris et al. 2004). Thus using a specific form of the spectrotemporal envelope may not allow us to capture the complete processing of a neuron. Third, the state of the animal may be a factor, since anesthesia, for example, may decrease the number of tonic responses and change inhibitory mechanisms (Astl et al. 1996; Lu et al. 2001; Versnel et al. 2009). This would affect the nature of the STRFs and nonlinearities, though not our ability to calculate them, since in the present study we were able to calculate filters for neurons that had tonic responses. Fourth, we presented the DMR at one mean intensity, although the responses to the DMR may change at different intensities. Earlier work showed varying STRFs for differing intensities (Lesica and Grothe 2008). This effect may be partially mitigated in the case of the DMR, since it covers a 40-dB dynamic range. Finally, further work needs to ascertain the predictive power of a single MID. Our present study cannot address this, since we did not present multiple repetitions of a single stimulus segment (Sharpee 2007). The repeats are required since predictions need to be evaluated relative to the inherent noise in the neural response (Brenner et al. 2000; Hsu et al. 2004; Sahani and Linden 2003).

Conclusion. Multidimensional receptive fields emerge along the auditory midbrain-to-forebrain pathway. To establish this, we first analyzed the phasic-tonic nature of ICC responses and verified that spike-triggered analyses were appropriate. The information from the STA was similar to the MID1 information, and the MID1 information was similar to the joint MID1 and MID2 information. These results generalized across all temporal response types; thus, in the ICC, a single spectrotemporal filter may adequately describe acoustic processing. In contrast, the auditory cortex requires a multifilter description. Therefore, receptive field dimensionality increases from midbrain to cortex.

ACKNOWLEDGMENTS

We thank Andrew Tan, Marc Heiser, Kazuo Imaizumi, and Benedicte Philibert for experimental assistance and Mark Kvale for the use of his SpikeSort 1.3 Bayesian spike-sorting software.

GRANTS

C. A. Atencio and C. E. Schreiner were supported by National Institutes of Health Grants DC-02260 and MH-077970, the Coleman Memorial Fund, and Hearing Research Inc. T. O. Sharpee was supported by an Alfred P. Sloan Fellowship, a Searle Scholarship, NIH Grants R01 EY-019493 and K25 MH-068904, the Ray Thomas Edwards Career Development Award in Biomedical Sciences, and the McKnight Scholarship. Computing resources were provided by the National Science Foundation (NSF) through TeraGrid resources provided by supercomputer resources at the San Diego Supercomputer Center, Argonne National Laboratory, University of Illinois National Center for Supercomputing Applications, and Texas Advanced Computing Center. Additional resources were provided by the Center for Theoretical Biological Physics (NSF PHY-0822283).

DISCLOSURES

No conflicts of interest, financial or otherwise, are declared by the author(s).

AUTHOR CONTRIBUTIONS

Author contributions: C.A.A., T.O.S., and C.E.S. conception and design of research; C.A.A. and C.E.S. performed experiments; C.A.A. and T.O.S. analyzed data; C.A.A., T.O.S., and C.E.S. interpreted results of experiments; C.A.A. prepared figures; C.A.A. drafted manuscript; C.A.A., T.O.S., and C.E.S. edited and revised manuscript; C.A.A., T.O.S., and C.E.S. approved final version of manuscript.

REFERENCES

Aertsen AM, Johannesma PI. The spectro-temporal receptive field. A functional characteristic of auditory neurons. *Biol Cybern* 42: 133–143, 1981.

Aitkin L. *The Auditory Midbrain: Structure and Function in the Central Auditory Pathway*. Clifton, NJ: Plenum, 1986.

Andoni S, Li N, Pollak GD. Spectrotemporal receptive fields in the inferior colliculus revealing selectivity for spectral motion in conspecific vocalizations. *J Neurosci* 27: 4882–4893, 2007.

Astl J, Popelar J, Kvasnak E, Syka J. Comparison of response properties of neurons in the inferior colliculus of guinea pigs under different anesthetics. *Audiology* 35: 335–345, 1996.

Atencio CA, Sharpee TO, Schreiner CE. Cooperative nonlinearities in auditory cortical neurons. *Neuron* 58: 956–966, 2008.

Atencio CA, Sharpee TO, Schreiner CE. Hierarchical computation in the canonical auditory cortical circuit. *Proc Natl Acad Sci USA* 106: 21894–21899, 2009.

Boyd S, Chua LO. Fading memory and the problem of approximating nonlinear operators with Volterra series. *IEEE Trans Circ Syst* CAS-32: 1150–1161, 1985.

Brenner N, Strong SP, Koberle R, Bialek W, de Ruyter van Steveninck RR. Synergy in a neural code. *Neural Comput* 12: 1531–1552, 2000.

Chen X, Han F, Poo MM, Dan Y. Excitatory and suppressive receptive field subunits in awake monkey primary visual cortex (V1). *Proc Natl Acad Sci USA* 104: 19120–19125, 2007.

David SV, Mesgarani N, Fritz JB, Shamma SA. Rapid synaptic depression explains nonlinear modulation of spectro-temporal tuning in primary auditory cortex by natural stimuli. *J Neurosci* 29: 3374–3386, 2009.

de Boer E, Kuyper P. Triggered correlation. *IEEE Trans Biomed Eng* 15: 169–179, 1968.

deCharms RC, Blake DT, Merzenich MM. Optimizing sound features for cortical neurons. *Science* 280: 1439–1443, 1998.

Ehret G. The auditory midbrain, a "shunting-yard" of acoustical information processing. In: *The Central Auditory System*, edited by Ehret G, Romand R. New York: Oxford Univ. Press, 1997, p. 259–316.

Elhilali M, Fritz JB, Klein DJ, Simon JZ, Shamma SA. Dynamics of precise spike timing in primary auditory cortex. *J Neurosci* 24: 1159–1172, 2004.

Escabí MA, Nassiri R, Miller LM, Schreiner CE, Read HL. The contribution of spike threshold to acoustic feature selectivity, spike information content, and information throughput. *J Neurosci* 25: 9524–9534, 2005.

Escabí MA, Schreiner CE. Nonlinear spectrotemporal sound analysis by neurons in the auditory midbrain. *J Neurosci* 22: 4114–4131, 2002.

Hsu A, Borst A, Theunissen FE. Quantifying variability in neural responses and its application for the validation of model predictions. *Network* 15: 91–109, 2004.

Huang CL, Winer JA. Auditory thalamocortical projections in the cat: laminar and areal patterns of input. *J Comp Neurol* 427: 302–331, 2000.

Johnson DH. The relationship between spike rate and synchrony in responses of auditory-nerve fibers to single tones. *J Acoust Soc Am* 68: 1115–1122, 1980.

Joris PX, Schreiner CE, Rees A. Neural processing of amplitude-modulated sounds. *Physiol Rev* 84: 541–577, 2004.

Klein DJ, Depireux DA, Simon JZ, Shamma SA. Robust spectrotemporal reverse correlation for the auditory system: optimizing stimulus design. *J Comput Neurosci* 9: 85–111, 2000.

Korenberg MJ. Parallel cascade identification and kernel estimation for nonlinear systems. *Ann Biomed Eng* 19: 429–455, 1991.

Kuwada S, Yin TC, Syka J, Buunen TJ, Wickesberg RE. Binaural interaction in low-frequency neurons in inferior colliculus of the cat. IV. Comparison of monaural and binaural response properties. *J Neurophysiol* 51: 1306–1325, 1984.

Lesica NA, Grothe B. Dynamic spectrotemporal feature selectivity in the auditory midbrain. *J Neurosci* 28: 5412–5421, 2008.

Lewicki MS. Bayesian modeling and classification of neural signals. *Neural Comput* 6: 1005–1030, 1994.

Liu LF, Palmer AR, Wallace MN. Phase-locked responses to pure tones in the inferior colliculus. *J Neurophysiol* 95: 1926–1935, 2006.

Lu T, Liang L, Wang X. Temporal and rate representations of time-varying signals in the auditory cortex of awake primates. *Nat Neurosci* 4: 1131–1138, 2001.

Malmierca MS, Saint Marie RL, Merchan MA, Oliver DL. Laminar inputs from dorsal cochlear nucleus and ventral cochlear nucleus to the central nucleus of the inferior colliculus: two patterns of convergence. *Neuroscience* 136: 883–894, 2005.

Marmarelis PZ, Marmarelis VZ. *Analysis of Physiological Systems: the White Noise Approach*. New York: Plenum, 1978.

Marmarelis VZ. Modeling methodology for nonlinear physiological systems. *Ann Biomed Eng* 25: 239–251, 1997.

Marmarelis VZ. *Nonlinear Dynamic Modeling of Physiological Systems*. New York: Plenum, 2004.

Merzenich MM, Reid MD. Representation of the cochlea within the inferior colliculus of the cat. *Brain Res* 77: 397–415, 1974.

Mitani A, Shimokouchi M, Itoh K, Nomura S, Kudo M, Mizuno N. Morphology and laminar organization of electrophysiologically identified neurons in the primary auditory cortex in the cat. *J Comp Neurol* 235: 430–447, 1985.

Morest DK. The laminar structure of the medial geniculate body of the cat. *J Anat* 99: 143–160, 1965.

Oliver DL. Ascending efferent projections of the superior olivary complex. *Microsc Res Tech* 51: 355–363, 2000.

Oliver DL. Neuronal organization in the inferior colliculus. In: *The inferior Colliculus*, edited by Winer JA, Schreiner CE. New York: Springer, 2005, p. 69–114.

Oliver DL, Beckius GE, Shneiderman A. Axonal projections from the lateral and medial superior olive to the inferior colliculus of the cat: a study using electron microscopic autoradiography. *J Comp Neurol* 360: 17–32, 1995.

Palm G. On representation and approximation of nonlinear systems. *Biol Cybern* 34: 49–52, 1979.

Rodriguez FA, Read HL, Escabi MA. Spectral and temporal modulation tradeoff in the inferior colliculus. *J Neurophysiol* 103: 887–903, 2010.

Rouiller EM, Simm GM, Villa AE, de Ribaupierre Y, de Ribaupierre F. Auditory corticocortical interconnections in the cat: evidence for parallel and hierarchical arrangement of the auditory cortical areas. *Exp Brain Res* 86: 483–505, 1991.

Rust NC, Schwartz O, Movshon JA, Simoncelli EP. Spatiotemporal elements of macaque v1 receptive fields. *Neuron* 46: 945–956, 2005.

Sahani M, Linden JF. How linear are auditory cortical responses? In: *Advances in Neural Information Processing Systems 15*, edited by Becker S, Thrun S, Obermayer K. Cambridge, MA: MIT Press, 2003, p. 109–116.

Schofield BR. Superior olivary complex and lateral lemniscal connections of the auditory midbrain. In: *The Inferior Colliculus*, edited by Winer JA, Schreiner CE. New York: Springer, 2005, p. 132–154.

Schreiner CE, Langner G. Laminar fine structure of frequency organization in auditory midbrain. *Nature* 388: 383–386, 1997.

Schreiner CE, Sutter ML. Topography of excitatory bandwidth in cat primary auditory cortex: single-neuron versus multiple-neuron recordings. *J Neurophysiol* 68: 1487–1502, 1992.

Schwartz O, Pillow JW, Rust NC, Simoncelli EP. Spike-triggered neural characterization. *J Vis* 6: 484–507, 2006.

Sharpee T, Rust NC, Bialek W. Analyzing neural responses to natural signals: maximally informative dimensions. *Neural Comput* 16: 223–250, 2004.

Sharpee TO. Comparison of information and variance maximization strategies for characterizing neural feature selectivity. *Stat Med* 26: 4009–4031, 2007.

Sharpee TO, Miller KD, Stryker MP. On the importance of static nonlinearity in estimating spatiotemporal neural filters with natural stimuli. *J Neurophysiol* 99: 2496–2509, 2008.

Sharpee TO, Sugihara H, Kurgansky AV, Rebrik SP, Stryker MP, Miller KD. Adaptive filtering enhances information transmission in visual cortex. *Nature* 439: 936–942, 2006.

Singh NC, Theunissen FE. Modulation spectra of natural sounds and ethological theories of auditory processing. *J Acoust Soc Am* 114: 3394–3411, 2003.

Strong SP, Koberle R, de Ruyter van Steveninck R, Bialek W. Entropy and information in neural spike trains. *Phys Rev Lett* 80: 197–200, 1998.

Touryan J, Lau B, Dan Y. Isolation of relevant visual features from random stimuli for cortical complex cells. *J Neurosci* 22: 10811–10818, 2002.

Treves A, Panzeri S. The upward bias in measures of information derived from limited data samples. *Neural Comput* 7: 399–407, 1995.

Versnel H, Zwiers MP, van Opstal AJ. Spectrotemporal response properties of inferior colliculus neurons in alert monkey. *J Neurosci* 29: 9725–9739, 2009.

Wang X, Lu T, Snider RK, Liang L. Sustained firing in auditory cortex evoked by preferred stimuli. *Nature* 435: 341–346, 2005.

Westwick DT, Kearney RE. Nonparametric identification of nonlinear biomedical systems. 1. Theory. *Crit Rev Biomed Eng* 26: 153–226, 1998.

Winer JA. Anatomy of layer IV in cat primary auditory cortex (AI). *J Comp Neurol* 224: 535–567, 1984.

Winer JA. The functional architecture of the medial geniculate body and the primary auditory cortex. In: *The Mammalian Auditory Pathway*, edited by Webster DB, Popper AN, Fay RR. New York: Springer, 1992, p. 222–409.

Winter IM, Palmer AR. Responses of single units in the anteroventral cochlear nucleus of the guinea pig. *Hear Res* 44: 161–178, 1990.